DISTRIBUTION STATEMENT A. Approved for public release; distribution is unlimited.

Completion of Graduate Student Work Funding Request: Bedform Parameterization and Object Detection from Autonomously Gathered Sonar Data- Application of a Fingerprint Algorithm System

PI: Arthur C. Trembanis
CSHEL
http://cshel.geology.udel.edu/CSHEL/
College of Earth, Ocean, and Environment
University of Delaware
109 Penny Hall
Newark DE, 19716
phone: (302) 831-2498 fax: (302) 831-4158 email: art@udel.edu

Award Number: N00014-14-1-0091

LONG-TERM GOALS

The long-range goals of this research are to improve our ability to characterize the seabed geometry and texture in energetic inner-shelf/bay mouth settings composed of heterogeneous sedimentary material with dynamic seabed ripples. Our purpose is to improve our understanding of bedform dynamics and spatio-temporal length scales and defect densities through the application of a recently developed fingerprint algorithm technique (Skarke and Trembanis, 2011) in the vicinity of manmade seabed objects and dynamic natural ripples on the inner shelf utilizing high-resolution swath sonar collected by an AUV and from surface vessel sonars in energetic coastal settings with application to critical military operations such as mine countermeasures.

OBJECTIVES

The overall objectives of this project are a sonar based (platform independent) bedform parameterization, refinement of the fingerprint algorithm tool-kit and testing of non-equilibrium ripple geometry models with field observations of ripples exposed to major storm events. This specific project provided direct funding for graduate student involvement in the project and the tasks and findings of the graduate student project are the focus of this report.

The following are the specific objectives of this funded project:

1. Extend and apply recently developed fingerprint algorithm techniques (Skarke and Trembanis, 2011) for ripple parameterization and object detection using AUV, ship, and rotary sonar derived backscatter and bathymetry data.
2. Providing direct funding for student involvement in the form of a graduate student RA to Carter DuVal for completion of MS thesis work based on the project data.
3. Comparative analysis of hydrodynamics to bedforms morphodynamics to capture spatial and temporal changes to the seabed, specifically storm event effects and recovery

4. Apply fingerprint algorithm (Skarke and Trembanis 2011) to side-scan sonar and multibeam backscatter to extract bedform length scales, orientation, and defect density (example from March 2013 dataset left).
5. Isolate spatial effects of seabed objects on ripple bedform morphodynamics and scour
6. Test and compare current non-equilibrium ripple models against Fingerprint Algorithm results

APPROACH

Our approach has been to obtain a suite of field observations by performing carefully repeated high-resolution seafloor mapping over a natural seabed system approximately 1-2 km's on a side including areas with dynamic ripple bedforms and manmade structures. We have gathered: (1) acoustic bathymetry and backscatter of surface sediment layers from an autonomous underwater platform and from surface vessel multibeam echosounder sonar; (2) small scale (sub-meter) optical imagery from a small maneuverable AUV platform, and; (3) further developed a remote acoustic segmentation and classification system (ARA) for bathymetry and backscatter data collected at the field site. We have also deployed and maintained a bottom-moored instrument package with an ADCP (waves and current) and rotary sonar (2D ripples) for time-series measurements of hydrodynamics and small-scale bedform dynamics (*sensu* Skarke and Trembanis, 2011). The fusion of these remotely sensed data (hydrodynamics and morphology) with ground truth samples and the ARA remote acoustic model were used to test existing ripple models and improve our understanding of the response of the seabed to mean and oscillatory flows (tidal and wave driven respectively) and the interpretation of acoustic imagery for surface textural properties of surficial sediments on the seabed in other settings.

WORK COMPLETED

The following section highlights the major research accomplishments from this project over the final year of the project covering the period from December 2013 – September 2014.

- Defect density algorithm improved for extraction of ripple minutiae structures (bifurcations and terminations)
- Added new sinuosity calculation to fingerprint algorithm tool-box.
- Comparative quantitative analysis conducted between fingerprint algorithm derived observations of ripple dimensions to those predicted from several widely used predictive analytical ripple models.
- 1 MS thesis and 1 undergraduate honors thesis completed and defended (S. Wang & C. DuVal); 2 additional MS theses (T. Metz and C. Englert) and 1 PhD (P. Kannappan) all supported by project data.
- 4 public presentations of project results including 3 invited seminars

RESULTS

<u>Bottom Mount Instrument Deployments</u>

The bottom mount consisted of the following instruments:

- 600 kHz upward looking ADCP with wave and current profiling capability
- 2.25 mHz Imagenex 881 rotary fanbeam sonar for time-series measurements of bedform planview geometry

Since onsite hydrodynamic data could not be recorded for a complete annual cycle with the instrument frame, observations were augmented by wave data from NOAA buoy 44009, as with the study conducted by Raineault et al., (2013). The buoy is situated 23 kilometers south of Redbird Reef, and is moored at a similar distance from the coast (30.5 km) and in similar water depth (30.5m). The buoy has been operational since 1984, and offers a nearly complete historical record of wave height and period since that time. Comparisons between buoy 44009 and Redbird ADCP significant wave height show an $r^2 = 0.958$ correlation, with the buoy recording slightly higher wave heights on average. During the research collection period, the buoy was down between Dec. 2012 and March 2013. NOAA WaveWatch3 (WW3) hind casting was used to fill in this gap. The Wave Watch 3 data under represents wave heights for the Redbird Reef area, so a linear transform was preformed to correct the difference. Comparison between the corrected WW3 and Redbird ADCP Hs show an $r^2 = 0.95$ correlation, with the WW3 corrected data being sufficient to complete the wave record.

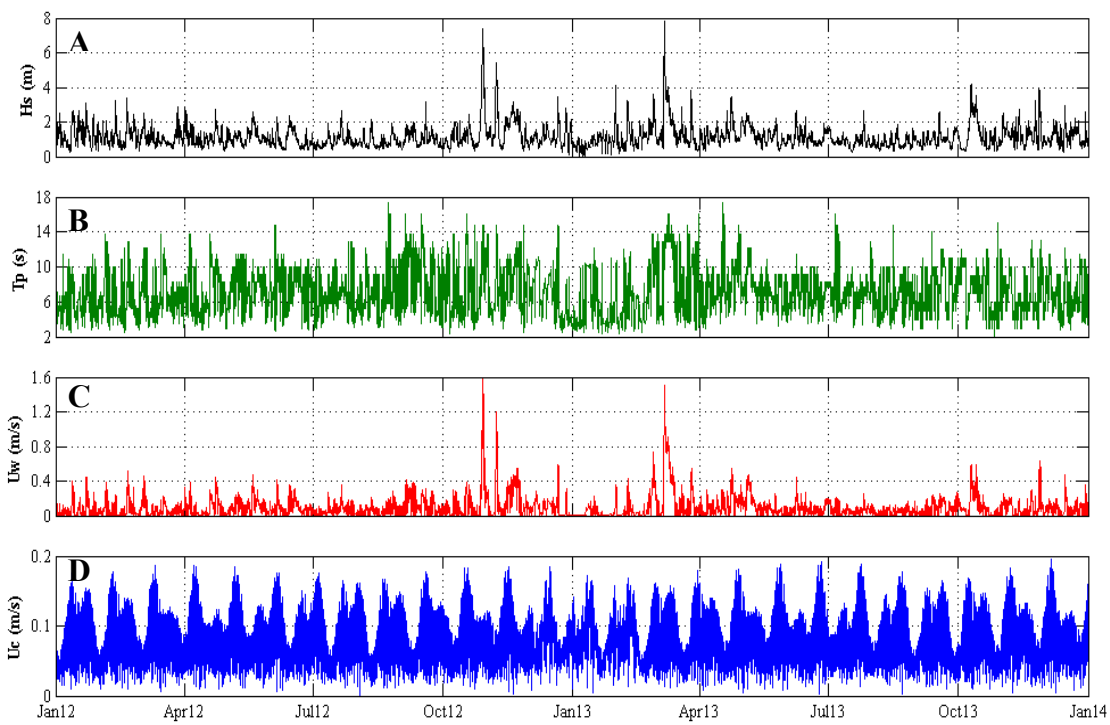

Figure 1: Composite hydrodynamic conditions (compiled using in situ ADCP, NOAA Buoy and WaveWatch III model hindcasts) from January 2012-2014. A) Significant wave height. B) Peak wave period. C) Near-bed significant orbital velocity. D) Near-bed tidal current predictions.

Hydrodynamic conditions were compiled and calculated from the combined buoy 44009 and Wave Watch 3 data from January 2012 through December 2013. Figure 1 shows the significant wave height (Hs), peak period (Tp), estimated bottom orbital velocity (Uw), and estimated tidal near bed current (Uc). Wave height averaged between 1.14 and 1.15 meters between with 2012 and 2013, while wave

period averaged around 7.3 second for both years. Annual mean orbital velocity averaged around 0.1 m/s for both years. These statistics are comparable to annual wave height, period and near-bed orbital velocity statistics calculated by Raineault et al. (2013) for the Redbird reef site from 2008 through 2011. Predicted tidal near bed currents ranged from 0.1 to 20 cm/s over both years, averaging around 7.7 cm/s. This compares favorably to measured ADCP near bed currents from the four deployments, which averaged 9.6 cm/s but ranged from less than 0.1 cm/s to over 50 cm/s due to storm event influence. Tidal harmonic analysis derived from the longest ADCP dataset indicated the semi-diurnal M2 as the major tidal force.

During the course of the study, three large storm events took place. Hurricane Sandy passed north of the reef on Oct. 28-29, 2012, generating wave heights measured over 7.1 meters (Hs) with peak period of 14-seconds at the site. This was followed by a nor'easter 7 days later, which generated waves over 4.8 meters with periods up to 14 seconds. The instrument mooring at the site, as well as buoy 44009, captured both events. The third storm event took place March 6-8, 2013, which generated waves up to 7.8 meters, again with peak periods of 14 seconds, as captured by buoy 44009. Estimated bottom orbital velocities peaked at over 1.5 m/s during hurricane Sandy, and nearly 1.2 m/s in the following nor'easter. Corresponding orbital velocity measurements derived from the bottom facing PC-ADCP showed orbital velocities 20 cm above the bed to be up to nearly 1.6 m/s for both Sandy and the following nor'easter. Superimposed on the orbital motion were mean bottom currents measured during the storms peaked at 73 cm/s and 63 cm/s respectively. Estimated orbital velocities for the March 2013 nor'easter reach over 1.5 m/s, with sustained orbital velocities between 0.5 and 1 m/s lasting for 72 hours after the storm. Shields parameter sediment threshold and shear stress values calculated for grain sizes determined from grab samples indicate high levels of fine grain sediment suspension and transport during the storm events. Furthermore, storm events were energetic enough to mobilize even the coarsest sediment classes found on the seabed forming large distinct scour patches in the lee of artificial structures on the seabed. In addition, the storm conditions rotated and/or destroyed several of the subway car structures at the site.

Defect Density

Fingerprint algorithm analysis was conducted for ripple defect densities (e.g. ripple bifurcations and terminations) spatially from the AUV sonar data. Spatial defect density distributions showed increased defect densities especially around the southern terminus of the ripple bedform field throughout the study. The lowest density values occurred throughout the largest ripple bedform field, while the highest values occur in the sporadic pockets of ripple bedforms around the reef objects in particular. Comparisons to ripple wavelength distributions show the highest densities to be in areas of smaller ripple wavelengths: the areas of the highest 10 percent defect densities are situated in areas with the mean wavelengths of 0.6 meters (versus mean values of 1.1 meters throughout the site). Results suggest there is an inverse relationship between ripple wavelengths and ripple defect densities. Skarke and Trembanis (2011) noted that effect of object scour could result in numerous small bedforms with shorter wavelengths, which, as they suggested, would appear as higher density regions of ripple defects. The data here supports this hypothesis, although in their study, Skarke and Trembanis (2011) found no distinct relationship between ripple wavelength and defect density. As well, they found higher defect densities associated with periods of poor bed definition, which is supported by the high defect densities in March 2013 backscatter where the ripples had undergone erosion.

Qualitative observations of defect density showed distinguishable increases in defect density ripple bedforms near reef objects. To determine whether there was a quantitative pattern concerning defect density relative to proximity and orientation to reef objects, three subway car test subjects were analyzed for proximal defect densities (Figure 2). The results indicate that defect densities in the proximity of the subway cars are not only greater than those than around the control point, but are also more variable. However, with respect to the affects of proximity, we see little variation between the ranges on the control points (standard deviation of 0.092 and 0.087 defects/m^2 for November 2012 and March 2013). With the subway cars, highest defect densities were found anywhere between 5 - 15 meters away, with wide distributions of defect density values. Standard deviations in defect density for Nov. 2012 and March 2013 were 0.14 and 0.2 defects/m^2 for the subway car in Figure 2. There is a tendency for lower values immediately next to the subway cars, where scour pits and acoustic shadows disrupt ripple measurements. Orientation with respect to the object appears to have little influence on variations in defect density: higher defect densities occur on every side of the objects. Regardless, the pattern of increased defect densities around artificial objects on the seabed warrants future considerations as this may provide a useful diagnostic tool to locating and characterizing seabed objects.

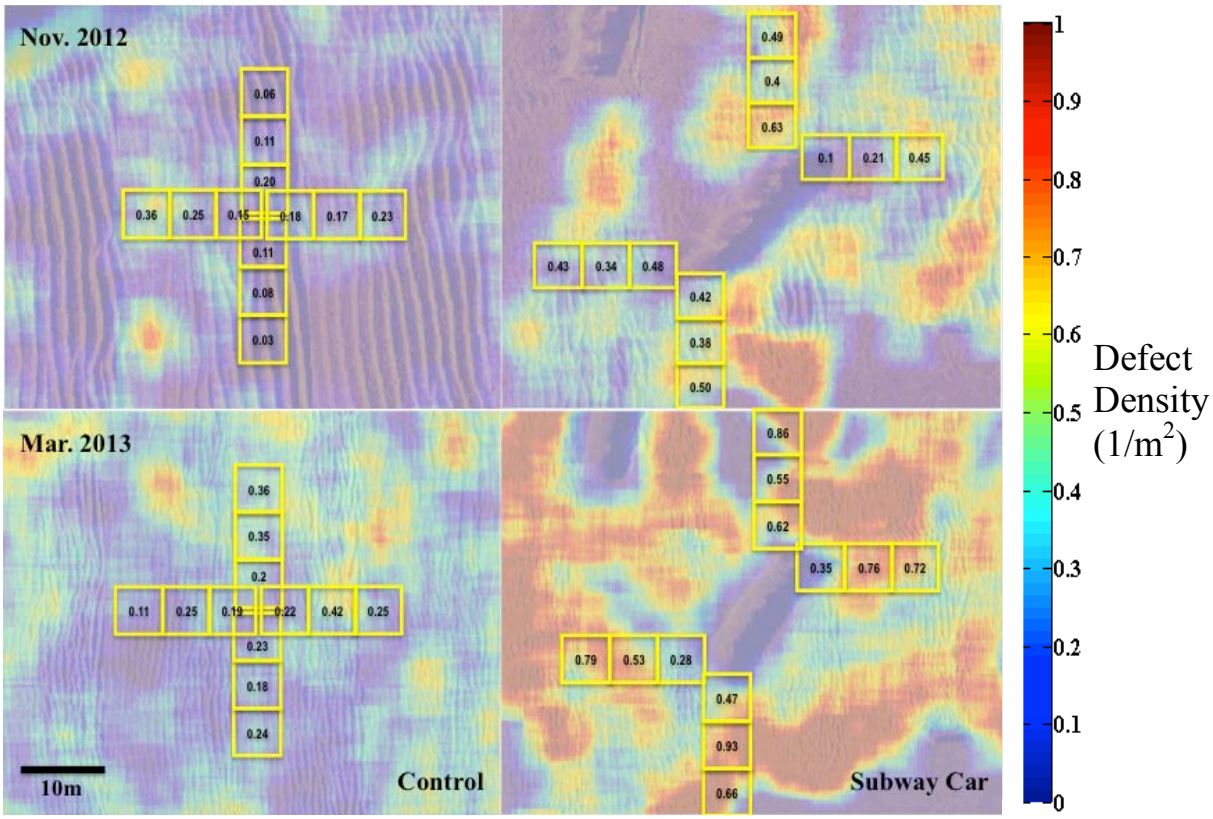

Figure 2: Defect density observations within a ripple bedform field (left) and around a subway car (right) for both the Nov. 2012 and March 2013 data sets. Note the higher densities around the reef object.

Fingerprint Algorithm Development

Since its release by Skarke and Trembanis (2011), the fingerprint algorithm has gone through several development updates and has become increasingly utilized by researchers examining small-scale ripple dynamics. The latest updates include improved defect density detection and a new algorithm for detecting ripple crest sinuosity (meandering). Previously, defect density calculations centered on ripple bifurcations, but termination defects were mainly excluded. The recent updates have now not only incorporated terminations, but permit the separate detection of bifurcations and terminations. These refinements allow for more explicit treatment of bifurcations and terminations as distinct geomorphic features. Furthermore, it allows for the exclusion of terminations at the edges of the fields, focusing only on those within the ripple field. This will serve as an important method to analyze bifurcations and terminations caused solely by natural ripple crest migration, as well as the potential to study small object effects (e.g. mines or unexploded ordnance) on ripple migration, specifically defect density.

A number of studies (e.g. Smyth and Li, 2005; Lacy et al., 2007) have suggested that orthogonal current and wave forcing may lead to increased ripple crest sinuosity. This, in turn, may affect ripple bedform migration and ripple defect generation and density (Faraci and Anderson, 2002). As such, we developed the sinuosity algorithm to work in conjunction with the defect detection suite to permit the subsequent analysis of the effects of flow on sinuosity and defect density. Figure 3 illustrates a typical sinuosity profile taken from Redbird Reef. Initial comparisons to defect density suggest defect density increases in areas of high sinuosity. Whether sinuosity, and in turn orthogonal forcing, are the cause of this pattern should be the subject of further future study.

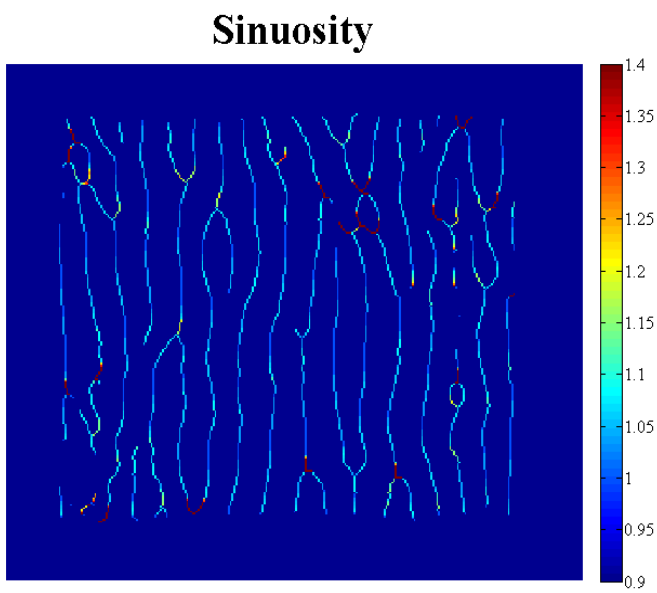

Figure 3: Ripple crest sinuosity from a ripple patch at Redbird Reef. Sinuosity is calculated by the ratio of ripple crest distance over the straight-line distance from start to finish. Areas with values increasingly greater than 1 are more sinuous.

Comparative Model Analysis

A comparative model analysis was conducted on time-dependent ripple geometric predictors, based of the Soulsby et al., (2012) non-equilibrium model. Recent studies (Soulsby and Whitehouse, 2005; Doucette and O'Donoghue, 2006; Traykovski, 2007; Voulgaris and Morin, 2008, Soulsby et al., 2012) have noted that established ripple bedforms could take significant amounts of time to react to changes in flow conditions. As such, the Soulsby model uses a generic derivative that incorporates either wave or current dominated conditions, and can be forced either by ripple wavelength, height or orientation calculations from equilibrium ripple models (i.e. synchronous hydrodynamic conditions) to produce asynchronous ripple geometric predictions. Three equilibrium models (Soulsby and Whitehouse, 2005; Traykovski, 2007; and Nelson et al., 2013) were selected and tested for comparison to fingerprint algorithm results. The models used grain size estimates generated from sediment samples collected at the sorted bedform field within the backscatter data analyzed with the fingerprint algorithm. Nine samples were chosen to help demonstrate predicted ripple geometric distributions from models versus calculated geometric distributions from the fingerprint algorithm.

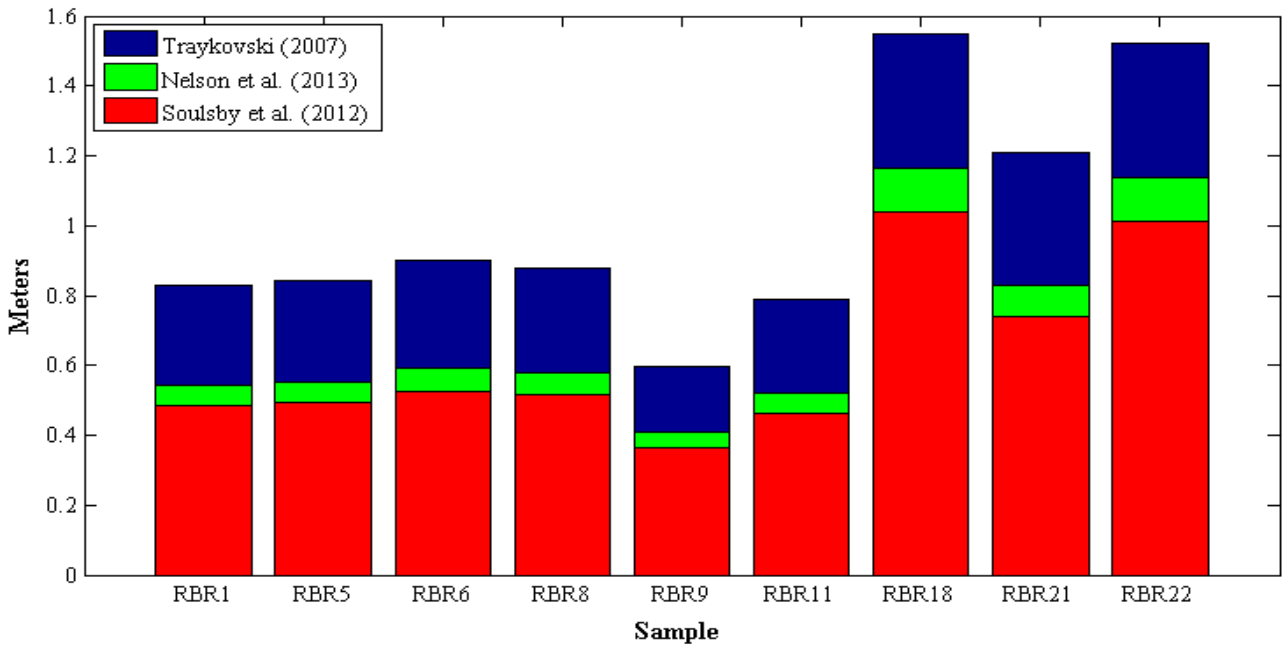

Figure 4: Ripple wavelength comparison after Hurricane Sandy between (blue) Traykovski (2007), (green) Nelson et al. (2013), and (red) Soulsby et al. (2012) for weighted mean sediment size.

The Soulsby et al. (2012) model (based on Soulsby and Whitehouse 2005 ripple equations) largely under predicted the ripple wavelength values (Figure 4). No ripple wavelengths were predicted greater than 1 meter, while 46.9 percent of the total ripple wavelength distribution from the fingerprint algorithm results was greater than 1 meter. Likewise, the Nelson et al., (2013) wavelength predictors under predicted, predicting no ripple wavelengths greater than 1.17 meters; thirty-three percent of the ripple distribution was greater than 1.17 meters. The Traykovski (2007) wavelength predictions were considerably higher than the other two models. The model predicted the largest ripple wavelength at 1.55 meters, with only 12 percent of the wavelength distribution falling above that prediction (Figure

4). Furthermore, the minimum wavelength prediction (0.6 meters) excluded only 8 percent of the wavelength distribution. Since the Traykovski (2007) equilibrium model encapsulated 80% of the wavelength distribution measured by the fingerprint algorithm, predictions in the study utilized the Traykovski (2007) model to analyze ripple pattern prior to our Nov. 2012, March 2013 and July 2013 AUV sonar surveys.

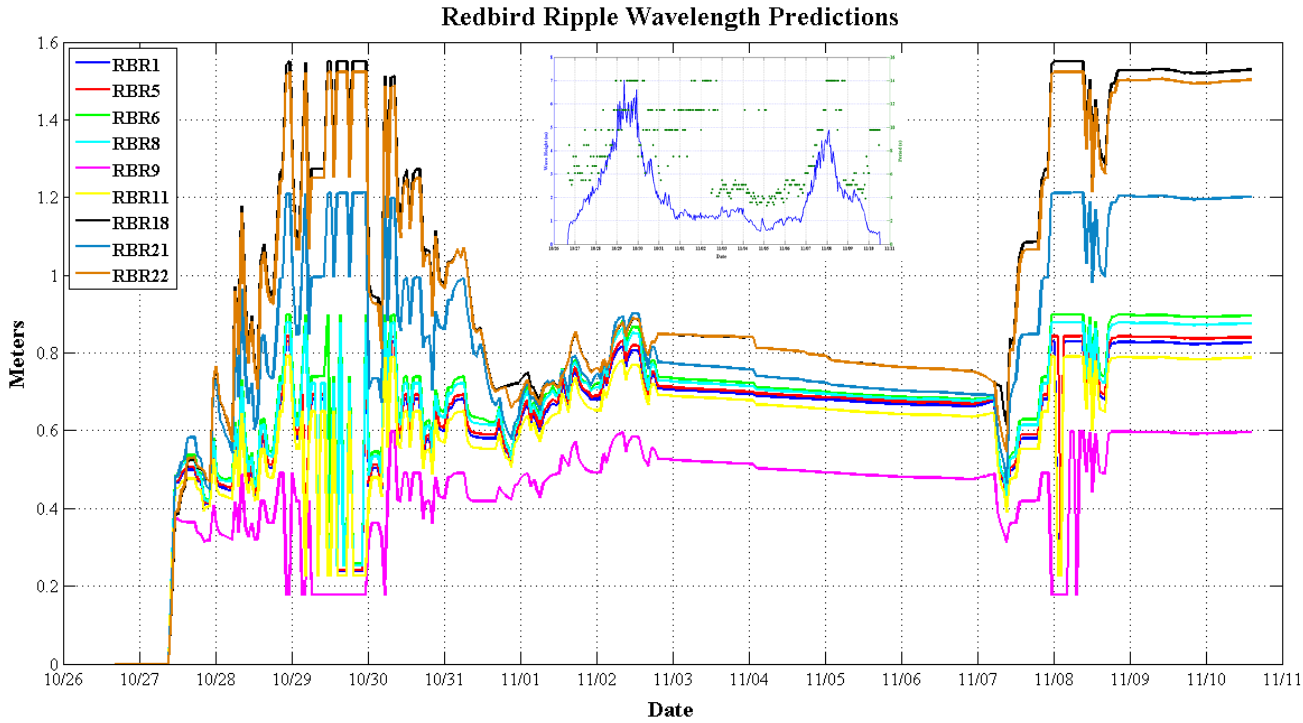

Figure 5: Non-equilibrium wavelength predictions from Oct. 26 to Nov. 10, 2012 showing the impacts of Hurricane Sandy and the nor'easter on ripple wavelength distribution. Subplot is Hs (blue) and Tp (green).

Non-equilibrium ripple predictions based on the ADCP data during Hurricane Sandy and nor'easter events indicated a high level of bedform activation and reorganization (Figure 5), as would be expected considering the changes found in pre- and post-Sandy sonar surveys. While direct hydrodynamic observations were unavailable prior to the March 29 and July 29, 2013 surveys, we estimated ripple wavelength and height values using wave data from NOAA Buoy 44009 and near-bed tidal current estimates. NOAA buoy and Redbird Reef Hs show an $r^2 = 0.956$ correlation and buoy near bed orbital velocity (Ub) estimates data have a strong correlation ($r^2 = 0.865$) with Redbird Reef ADCP Ub estimates. Using the buoy estimates, non-equilibrium ripple predictions can be modeled at the Redbird Reef over much larger time-spans (Figure 6). Likewise, this allowed us to estimate the ripple geometric conditions prior to the March and July 2013 surveys.

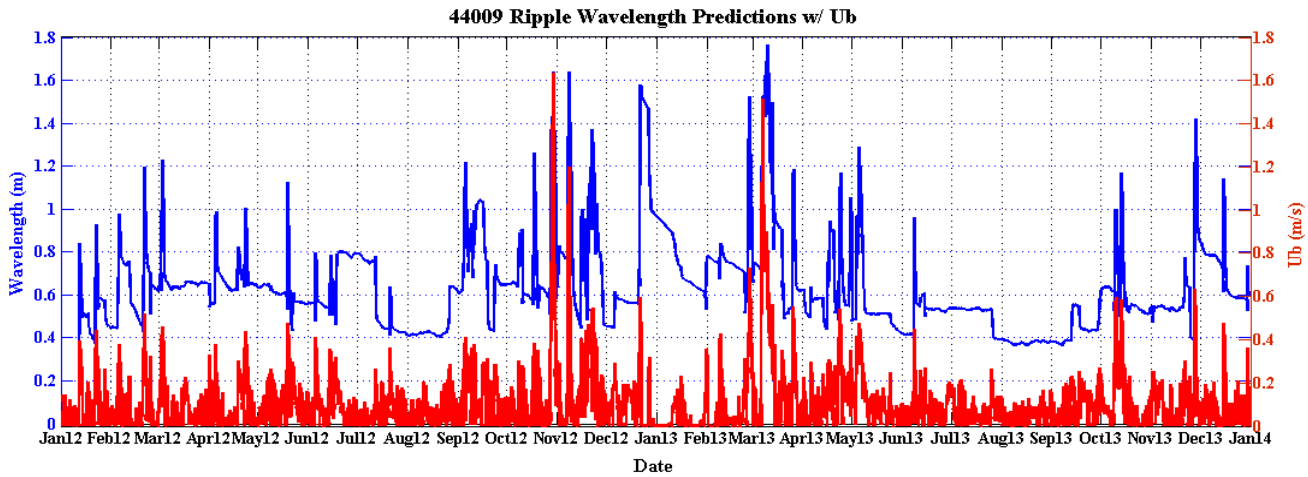

Figure 6: Non-equilibrium wavelength (blue) and wave orbital velocity (red) predictions from based on buoy 44009 wave conditions.

Figure 6 shows the coarsest sample (d50 ~ 1 mm) wavelength prediction over a 2012-2014 timespan. The model estimates a ripple reactivation between the March nor'easter and the March 29 survey, with peak ripple values topping out around 1 meter. Fingerprint algorithm statistics shows that only 8 percent of ripple wavelengths fell above 1 meter. However, the model indicates bedform wavelength decay for the coarsest sample at the time of the geoacoustic survey to only 0.62 meters, for which over 52 percent of the wavelength distribution was greater. Likewise, the largest predicted wavelength value at the time of the July survey was only 0.42 meters, having dropped off from over 0.5 meters only days before due to conditions just above critical threshold. This estimate is lower than 99 percent of the ripple wavelength distribution.

Thus, a discrepancy was found between the fingerprint algorithm and non-equilibrium model wavelength predictions. Further analysis indicated that the last peak storm predictions that occurred prior to the surveys match well with the fingerprint algorithm distribution, not predictions concurrent to the geoacoustic survey. For example, the wavelength predictions from the small event that took place just prior to the March 29, 2013 survey and after the March 5 nor'easter are also a strong match to the Fingerprint Algorithm distribution: only 8 percent of the recorded wavelengths were greater than the 1 meter prediction, and 11.2 percent were less than the smallest prediction. Other studies (e.g. Voulgaris and Morin, 2008) have found that the relict ripple wavelengths after storm events appeared to be the maximum wavelengths generated by the storms. The results from this comparison support the hypothesis that bedform conditions reflect non-contemporaneous energy levels reflective of waning periods of storms.

TRANSITIONS

Data products from this project are now being used by several other researchers in extension of this project including an MS student (C. Lawson) of Dr. Diane Foster and also by Dr. Brian Calder at UNH. Already this project has formed the basis of 3 existing MS student thesis projects (C. DuVal MS Oceanography UD 2014; T. Metz MS Geology expected Fall 2014; C. Englert MS UNH expected summer 2014) and one PhD (P. Kannapan, Mechanical Engineering UD expected 2016). The continued development and refinement of the ripple fingerprint algorithm code has been conducted in

partnership with A. Skarke (Mississippi State University) with the objective to host and make available to the research community fully documented version controlled code with detailed examples of implementation of the fingerprint algorithm code.

This project enhanceed existing ONR sponsored Mine Burial and Mine Countermeasure research by incorporating additional detailed field observations utilizing sonar systems from both a surface ship and a small portable AUV. The application of the recently developed fingerprint algorithm technique for bedform parameterization (Skarke and Trembanis, 2011) to bedform characterization provides a novel tool for object detection with impact to mine countermeasures.

RELATED PROJECTS

This project builds off of our directly related ONR Award Number N000141210303 and previous project N00014-07-1-0666 by Mayer and Trembanis. Benthic Hardbottom Mapping in DE Bay-NOAA Sea Grant (Trembanis- Co-PI). This project first introduced us to the Redbird reef site offshore of Delaware Bay and allowed us to conduct reconnaissance surveys of the seabed in this area between 2008-2011.

REFERENCES-

Doucette, J.S., and O'Donoghue, T., 2006. Response of sand ripples to change in oscillatory flow. Sedimentology 53, 581-596.

Faraci, C., and Andersen, K.H., 2002. Experimental Study on Ripple Patterns Generated by Combined Waves and Currents. 28th Convengo di Idraulica e Costruzioni idrauliche. September 16-19, 2002, Potenza.

Lacy, J.R., Rubin, D.M., Ikeda, H., Mokudai, K., and Hanes, D.M., 2007. Bed forms created by simulated waves and currents in a large flume. Journal of Geophysical Research-Oceans 112, C10018.

Mayer, Larry A., R. Raymond, G. Glang, M. D. Richardson, P. A. Traykovski, and A. C. Trembanis, 2007. High-resolution mapping of mines and ripples at the Martha's Vineyard Coastal Observatory, 2007. IEEE Journal of Oceanic Engineering, vol 32, no 1, pp 133-149.

Nelson, T.R., Voulgaris, G., and Traykovski, P. 2013. Predicting wave-induced ripple equilibrium geometry. J. of Geophys. Research – Oceans 118, 3202-3220.

Raineault, A.C. Trembanis, and D. Miller. 2011. Mapping benthic habitats in Delaware Bay and the coastal Atlantic: acoustic techniques provide greater coverage and high resolution in complex shallow water environments. Estuaries and Coasts. doi:10.1007/s12237-011-9457-8

Skarke, A., and A.C. Trembanis, 2011. Parameterization of bedform morphology and defect density with fingerprint analysis techniques. Continental Shelf Research, 31: 1688-1700.

Smyth, C.E., and Li, M.Z., 2005. Wave-current bedform scales, orientation, and migration on Sable Island Bank. Journal of Geophysical Research-Oceans 110, C02023.

Soulsby, R.L., Whitehouse, R.J.S., 2005. Prediction of ripple properties in shelf seas. Mark 1 predictor, Report TR150. HR Wallingford Ltd. UK for the ONR Ripples DRI Program.

Soulsby, R. L., R. J. S. Whitehouse, and K. V. Marten (2012), Prediction of time- evolving sand ripples in shelf seas, Cont. Shelf Res., 38, 47-62.

Traykovski, P., 2007. Observations of wave orbital scale ripples and a non-equilibrium time-dependent model. Journal of Geophysical Research-Oceans 112, C06026.

Voulgaris, G, and Morin, J.P., 2008. A long-term real time sea bed morphology evolution system in the south Atlantic Bight. Proceedings of the IEEE/OES/CMTC Ninth Working Conference on Current Measurement Technology, March 17-19, 2008, Charleston, SC.

PUBLICATIONS AND PRESENTATIONS OF RESULTS

Trembanis, A.C., C. DuVal, J. Beaudoin, V. Schmidt, D. Miller and L. Mayer, 2013. A detailed seabed signature from hurricane sandy revealed in bedforms and scour. Geochemistry, Geophysics, Geosystems Accepted manuscript online: 23 AUG 2013. DOI: 10.1002/ggge.20260

DuVal, C. and A.C. Trembanis, 2013. Hurricane Sandy's Fingerprint: Ripple Bedforms at an Artificial Reef. Dec. 2013. American Geophysical Union Fall Meeting Poster Session San Francisco, CA.

DuVal, C. and A.C. Trembanis, 2013. Object Scour and Bedform Dynamics at an Artificial Reef. Department of Geological Sciences Poster Seminar February 21, 2013.

Trevor Metz, A. C. Trembanis, John Madsen, and C. DuVal. Consideration of Shallow Stratigraphy for an Offshore Wind Farm, Symposium 2014, Lewes, DE.

Trembanis, A.C. Inner Shelf Scour and Bedform Dynamics from hurricane Sandy. University of Rhode Island Graduate School of Oceanography. Seminar October 24th, 2013.

Trembanis, A.C. Inner shelf bedform dynamics and scour associated with hurricane Sandy- impacts at artificial reef sites. University of Maryland Center for Environmental Studies, Horn Point Lab. Invited seminar Oct 23rd, 2013.

Trembanis, A.C. Drinking from the Firehose: strategies and techniques for dealing with large and noisy datasets. Examples from crowd sourcing image analysis and Phase Measuring Bathymetric Sonars (PMBS). AUV Users Conference. Lerici Italy October 15, 2013.

A.C. Trembanis, 2013. Sandy's Fingerprint: Inner Shelf, Barriers, and Beach Nourishment. AAPG Annual Convention and Exhibition. Special invited session: hurricane sandy and our vulnerable developed coastlines (Eastern section SEPM). Pittsburgh May 21, 2013.

A.C. Trembanis, 2013. Benthic habitat and seafloor morphology mapping. Stony Brook University School of Marine and Atmospheric Sciences. Ocean and Atmosphere Colloquim Seminar May 10, 2013.

A.C. Trembanis, 2013. Impacts of Hurricane Sandy on the Delaware Inner Shelf- Observations of Bedform Dynamics and Scour from the Redbird Reef Site. Physical Ocean Science and Engineering Seminar, April 26, 2013

DuVal, C. and A.C. Trembanis, 2013. Object Scour and Bedform Dynamics at an Artificial Reef. Department of Geological Sciences Poster Seminar February 21, 2013.

Student Involvement:

While there had been no previous direct student funding support in the related project budget, this particular project provided direct funding support to MS student Carter DuVal and helped to facilitate several graduate students theses and participation by more than a dozen undergraduates through our research cruises. Specifically the following 4 graduate students theses involve some component of the project data: 1) Carter DuVal MS Oceanography UDel; 2) Trevor Metz MS Geology UDel; 3) Christopher Englert MS UNH; 4) Prasanna Kappannan PhD Mech Eng UDel. Additionally NSF REU summer intern Seaver Wang (UPenn) developed and completed both his summer internship and senior honors thesis utilizing project related data.

Collaborative Partners:

This project has both built upon existing collaborations and lead to the development of new collaborations with the following colleagues- Giuseppe Masetti, University of New Hampshire, Doug Miller, University of Delaware; Bert Tanner, University of Delaware; Mark Moline, University of Delaware; Tobias Kukulka, University of Delaware; Doug Levin, Washington College; and Steve Donohue, EPA